A Demonstration of Frequency-Based Modulation for Underwater Optical Wireless Communication

(Invited paper)

Jianhui Chen, Callum T. Geldard, and Wasiu O. Popoola

School of Engineering, Institute for Digital Communications,
The University of Edinburgh, Edinburgh EH9 3JL, U.K.

Wasiu O. Popoola, w.popoola@ed.ac.uk

Abstract: *This paper presents experimental comparison of frequency-shift chirp modulation (FSCM), and frequency-shift keying (FSK), implemented using subcarrier intensity modulation (SIM) for underwater optical wireless communications (UOWC), in a range of channel conditions. Due to the nature of the UOWC, its channel poses difficulties in designing a reliable link in real-world water conditions. These channel effects include turbidity and turbulence, caused by suspended particles and channel inhomogeneities within the UOWC channel, respectively. Turbidity results in photon scattering and absorption while turbulence causes fluctuation and fading in the received signal amplitude. Encoding data on the frequency of the transmitted signal, as in FSCM and FSK, can protect data from these channel effects. The two techniques use different signal structures to implement frequency-based modulation. In FSK, data is encoded on the subcarrier frequencies of a SIM-modulated signal. Whereas in FSCM, data is carried within a chirp pulse encompassing a range of frequencies. In this paper, the performance of FSCM and FSK is evaluated in three different water conditions, these are: clear tap water; turbid water; and turbulent water, where both temperature inhomogeneity and air bubble induced turbulence effect are considered. The UOWC channel is first characterised to understand the effect of the various channel conditions on the propagating optical signal. Secondly, the power spectral density (PSD) is used to demonstrate how the frequency characteristics of the signal are affected by different channel conditions. Finally, the data performance of the two modulation schemes is compared in terms of the bit error rate (BER) and maximum achieved data rate. Experimental results show that both FSCM and FSK have resilience against the effect of turbulence and provide good performance in low signal-to-noise ratio underwater channel conditions. Further, it is shown that in the channel conditions considered, FSCM can achieve a higher maximum data rate compared to FSK.*

1. INTRODUCTION

The field of underwater optical wireless communication (UOWC) continues to attract attention due to its potential for low latency links and high data rates over short link ranges, in contrast to the dominant underwater acoustic communications (UAC) [1]. Wireless connectivity underwater has diverse applications in commercial, military, and civilian fields. These applications include underwater facility monitoring, oil exploration, and underwater archaeology [2]. The nature of UOWC makes it well suited to forming part of a hybrid network alongside UAC and radio-based systems.

However, the data carrying optical signal is affected by the underwater channel conditions that could lead to data transmission error. To offer resilience against some of the hostile channel effects, subcarrier intensity modulation (SIM) with frequency shift keying (FSK) has been reported in UOWC [3][4]. This paper further develops the idea of frequency-based UOWC by presenting an experimental demonstration of frequency shift chirp modulation (FSCM) with SIM. The performance of FSCM is then compared with that of FSK-SIM in different underwater conditions in a lab-based experiment.

2. BACKGROUND

2.1. THE UOWC CHANNEL

There are two main challenges to overcome in the UOWC channel, one is water turbidity and another is underwater turbulence [5]. Underwater turbidity is caused by the particles and impurities along the propagation path of UOWC link. These suspended particles cause the transmitted optical signal to be absorbed or scattered as they propagate the UOWC channel. This has the effect of decreasing the received optical power, and can result in an temporal spread in the received signal due to multiple scattering of photons. Whereas, underwater turbulence is caused by changing channel conditions (e.g. salinity, air bubbles and temperature) along the UOWC propagation path [6]. These changes in turn cause the refractive index along the link to fluctuate, causing the beam to deviate from its original trajectory. The resultant fluctuations in the received optical intensity, I, can be quantified by the scintillation index (SI), σ_I^2, as [1]:

$$\sigma_I^2 = \frac{\langle I^2 \rangle - \langle I \rangle^2}{\langle I \rangle^2}, \tag{1}$$

where $\langle . \rangle$ represents the ensemble average. A higher value of σ_I^2 means there is a greater degree of turbulence induced fading within the channel.

2.2. FREQUENCY-BASED MODULATION SCHEMES

The time continuous transmitted optical power in a UOWC system using intensity modulation with direct detection (IM/DD) can be described as [7]:

$$P_t(t) = P_{ave}(1 + \beta m(t)), \tag{2}$$

where P_{ave}, β ,and $m(t)$ are the average transmitted power, modulation index, and electrical signal carrying data respectively. When there is turbulence in the channel, the received optical

power will fluctuate. Meaning that data encoded on the amplitude of $m(t)$, as in pulse amplitude modulation (PAM), will be difficult to decode [3]. In multi-carrier SIM, $m(t)$ with N subcarriers is given as [7]:

$$m(t) = \sum_{i=1}^{N} A_i \cos(2\pi f_i t + \phi_i), \tag{3}$$

where A_i, f_i, and ϕ_i respectively denote the amplitude, frequency ,and phase of the i^{th} subcarrier. When the signal propagates through a channel that is affected by turbulence induced fading, A_i will vary but f_i and ϕ_i will not. This inherent resilience is exploited by encoding data on the frequency (and/or phase) of the subcarrier signal.

In the SIM with FSK scheme, data is encoded onto the frequency of a subcarrier. Here, each symbol is made up of $N = M$ subcarriers, where M is the modulation order, with the frequency of the active subcarrier representing the data to be transmitted during a symbol duration. For the SIM with FSCM on the other hand, a data symbol is represented by a frequency chirp signal that occupies the entire modulation bandwidth. That is, data is encoded on a sweep of frequencies, rather than just one subcarrier [8]. The symbol structure of FSCM has potential advantages over FSK that can make it more resilient to hostile channel effects in UOWC. The power efficiency of both FSCM and FSK has been compared for terrestrial optical wireless communication (OWC), showing that the symbol structure of FSCM is more efficient and results in a lower signal-to-noise ratio (SNR) requirement than FSK [9].

Additionally, the unique advantage of SIM-chirp signaling arises from the symbol energy not being concentrated in a single frequency of the subcarrier signal but spread across a progressively increasing range of frequencies within the symbol duration. As a result, the entire energy of a data symbol is 'shielded' from severe attenuation suffered by any single signal frequency. Thus, 'spreading' the symbol energy over a range of subcarrier signal frequencies with chirp signaling offers resilience to the combined effects of the channel and limitation of the front-end devices.

3. EXPERIMENTAL EVALUATION OF SIM WITH FSK AND FSCM

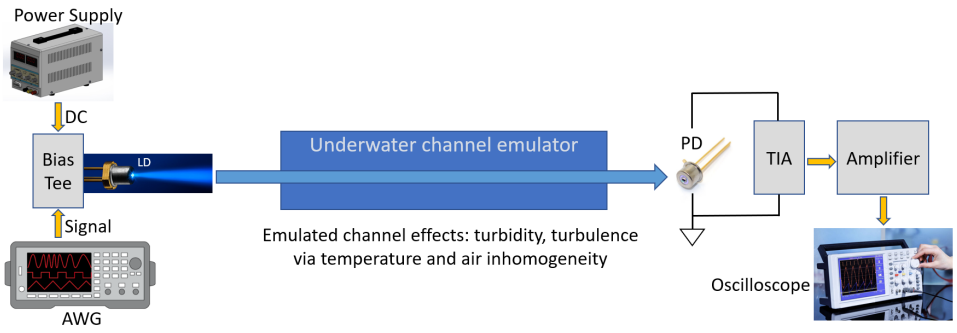

Figure 1: The system block diagram of experimental setup, including the laser diode (LD); Arbitrary waveform generator (AWG); Power supply; Photodiode (PD); Transimpedance amplifier (TIA); Oscilloscope

Figure 1 illustrates the block diagram of the experimental setup utilized in this study, including the underwater channel emulator (UCE). The data is first encoded by using FSK or

FSCM in MATLAB and then transmitted using a Keysight m8195a arbitrary waveform generator (AWG). To ensure the signals are positive and unipolar before transmission through Osram PL450b laser diodes (LD), a direct current (DC), is added via a bias-T. The optical signal then propagates through the UCE in which the water conditions can be controlled to emulate the underwater channel. At the receiver (Rx), the optical signal is converted into the electrical domain using a P-i-N photodiode (PD) with a TIA circuit. The signal is then amplified before being sampled using a digital oscilloscope (DSA90804A) and processed offline in MATLAB. The PD's has a -3 dB bandwidth of 1 GHz, this limits the overall modulation bandwidth of the experimental set-up.

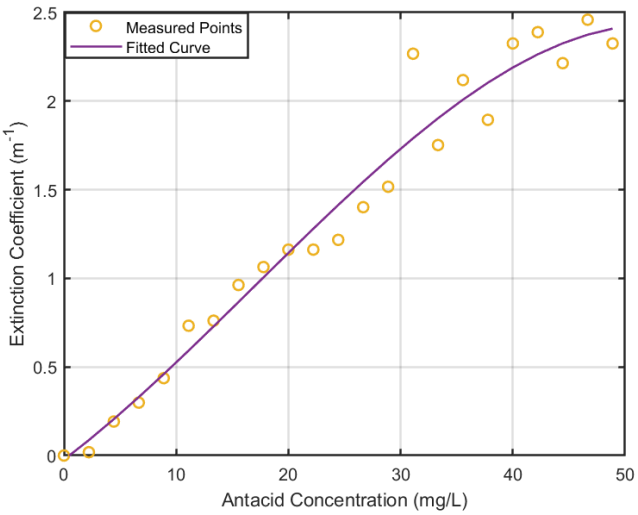

Figure 2: Estimated channel coefficients plotted against antacid concentration [5]

The UCE consists of a tank with dimensions $1.5 \times 0.5 \times 0.5$ m^3 in which the water conditions can be controlled. The UCE is filled with 210 L of clear tap-water, antacid tablets are used to control the water turbidity. The estimated extinction coefficients have been measured in [5] and is presented in Figure 2. When designing an experimental study in the laboratory, it is important to ensure that the channel conditions relate to a real-world scenario. To that end, the extinction coefficients used in this study are related to those observed in Jerlov's in-situ experiments and calculated in [10][11]. The approximate corresponding Jerlov water types, antacid concentrations considered, and extinction coefficients, denoted by $c(\lambda)$, in this experiment are illustrated in Table 1.

Turbid Level	Antacid Concentration (mg/L)	$c(\lambda)$ (m^{-1})	Approximate Jerlov Water Type [10]
Turbid 1	4.76	0.2	Jerlov IB
Turbid 2	16.7	0.8	Jerlov 3C
Turbid 3	28.6	1.5	Jerlov 5C

Table 1: Turbid parameters considered in experiments

Turbulence is produced in the UCE by introducing a temperature gradient along the link with a heating element, and monitored using the same process as described in reference [12]. This experimental study considers four different turbulent channel conditions: still water with $\sigma_I^2 \approx 0$; turbulent condition 1 with $\sigma_I^2 \approx 0.10$; turbulent condition 2 with $\sigma_I^2 \approx 0.17$; and turbulent condition 3 with $\sigma_I^2 \approx 0.24$. Bubble induced turbulence is generated by an air pump

with four ports that produce a total air amount of 15.0 L/min. This experiment employs a pipe divider to allocate flow rates from half, three quarters, one, and one pump port, producing bubbles with corresponding rates of 1.875 L/min, 2.813 L/min, and 3.75 L/min through the channel, resulting in corresponding turbulent conditions: turbulent condition 1 with $\sigma_I^2 \approx 0.10$; turbulent condition 2 with $\sigma_I^2 \approx 0.16$; turbulent condition 3 with $\sigma_I^2 \approx 0.23$. As turbulence is a random process, the values of σ_I^2 vary by around ± 0.03 throughout the course of this experiment. All of the turbulence conditions considered have $\sigma_I^2 < 1$ and are therefore in the weak turbulence regime.

4. CHANNEL CHARACTERISATION

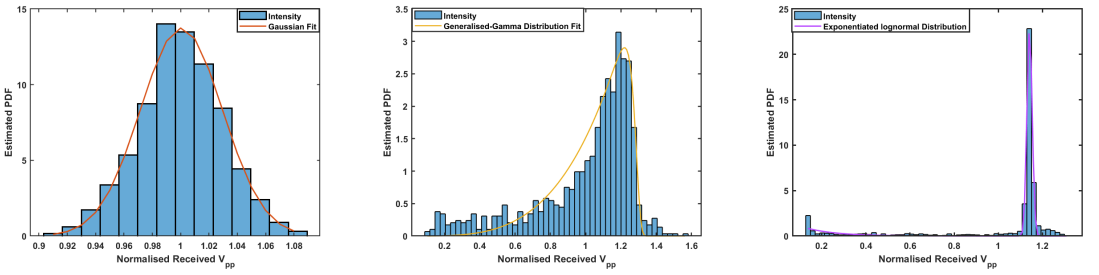

(a) Still water, $\sigma_I^2 \approx 0$

(b) Temperature turbulent water, $\sigma_I^2 \approx 0.10$, $\Delta T \approx 6$ K

(c) Bubble turbulent water, $\sigma_I^2 \approx 0.10$, $FR \approx 1.88$ L/min

Figure 3: Histogram showing the estimated probability density function (PDF) of the received V_{pp} in still, temperature and bubble turbulent water

The received intensity distributions and measured SI in both still and turbulent water are depicted in Figure 3. As expected, the received signal in still water conforms to a Gaussian distribution as illustrated in Figure 3a. On the other hand, the distribution in turbulence induced by temperature inhomogeneity fits a generalized Gamma distribution, as proposed in [13]. For bubble-induced turbulence, the received signal fits an exponential log-normal distribution, as proposed in [14]. The SI of the fitted distributions, σ_{fit}^2 and the corresponding coefficient of determination, R^2 are presented in Table 2, with the R^2 metric of fit being greater than 0.9 which indicates that they provide a good description of the data. Additionally, the Gaussian shape in still water is centred around mean of 1, indicating that the shape is dominated by noise in the system. When temperature induced turbulence is present, the shape of generalised Gamma distribution skews to the right, but the tail is fairly long towards 0, which means the channel varies a lot within the range. This fading will affect the received signal, leading a severe degradation to the UOWC.

As for the bubble induced turbulence, the exponential log-normal shape mainly gets some components at around 0.1 and a peak centred around 1.15. This suggests that bubble causes a deep fading event. This can be attributed to the fact that the bubble size is much larger than the wavelength of laser light, so the light beam is refracted and not scattered. As such, when the signal makes it to the receiver after refraction, the range of the received signal is less compared to the case of temperature temperature inhomogeneity induced turbulence.

Turbulence Type	Distribution Type	SI of Fit, σ^2_{fit}	Fitting Parameter
Still (no turbulence)	Gaussian	0.0008	$R^2 = 0.98$
Temperature fluctuation	Generalised Gamma [13]	0.0332	$R^2 = 0.93$
Bubble induced	Exponential Log-normal [14]	0.0394	$R^2 = 0.99$

Table 2: The fitting parameters for fitted curve in Figure. 3

5. DATA TRANSMISSION AND PERFORMANCE EVALUATION

In this section, the performance of FSCM and FSK-SIM is compared experimentally, in the previously described UOWC channel conditions. Figure 4 presents the BER against symbol rate for FSCM and FSK with $M = 2, 4, 8, 16$. For both FSK and FSCM, as the modulation order increases, symbol rate at which the BER exceeds the forward error correction (FEC) limit of 3×10^{-3} decreases expectedly. Below the FEC, coding techniques can be applied to make the transmission effectively error free. When the modulation order is 2, the BER curves of FSCM and FSK are close to each other, indicating that 2-FSCM has a similar performance with 2-FSK. However, when the M is higher than 2, there are more subcarriers available in each symbol, and the advantages of using FSCM become apparent. Specifically, FSCM consistently achieves a higher symbol rate than FSK at modulation levels of 4, 8 and 16. The results are in-line with the expectation based on the description of FSCM and FSK in Section 2.

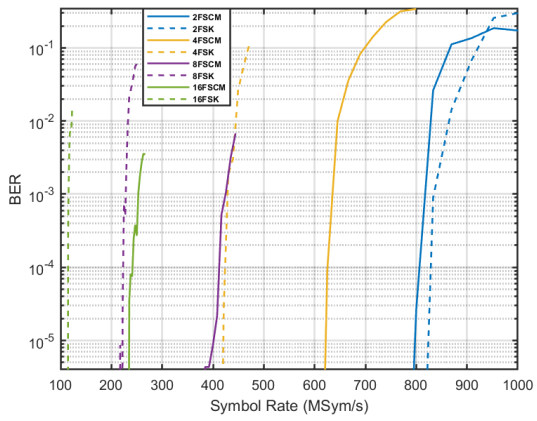

Figure 4: BER against symbol rate for M-FSK and M-FSCM in still water

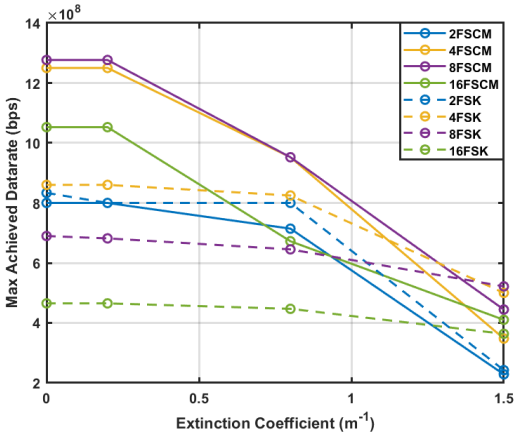

Figure 5: Performance of M-FSK and M-FSCM in different turbidity levels

Figure 5 gives the comparative results between FSCM and FSK in the 3 conditions of turbid water described in Section 3 in terms of the maximum data rate which can be achieved. The turbidity of a channel can be charaterised in terms of the extinction coefficients, the extinction coefficients are defined as the probability that a photon will experience interaction over link distance. As the extinction coefficients increase beyond 0.2 m^{-1}, the data rate falls as the received power decreases. When extinction coefficient is less than 0.2 m^{-1}, the maximum data rate is 1.25 Gbps achieved with 8-FSCM, compared to a maximum of 850 Mbps achievable with 4-FSK. However, as turbidity increases, the performance of FSCM degrades faster than that of FSK and becomes similar with FSK. At a extinction coefficient of 1.5 m^{-1}, 4,8-FSK achieves the maximum data rate at around 560 Mbps, while 2-FSK and 2-FSCM have the lowest data rates at about 210 Mbps. It can be concluded that both techniques will suffer from decreasing SNR due to turbidity, but FSK can maintain a more robust data transmission performance than

FSCM under low SNR conditions.

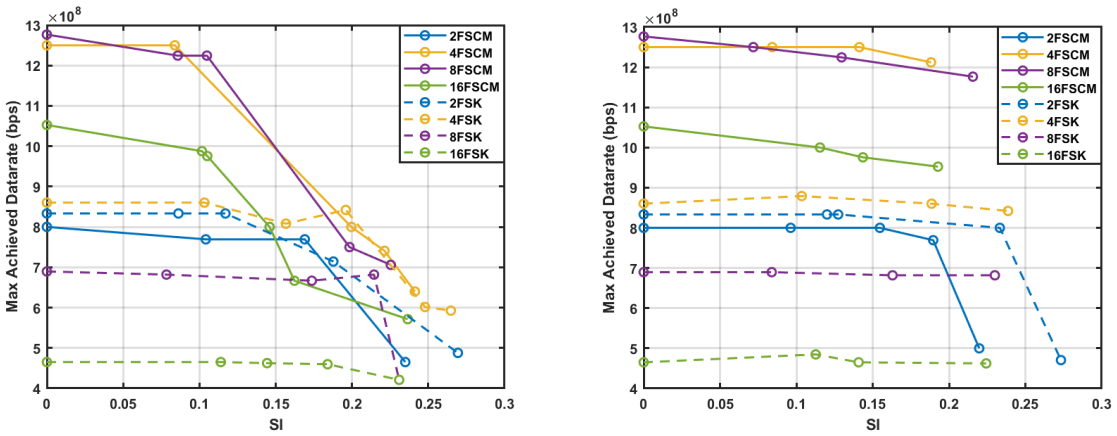

(a) Temperature turbulent water *(b) Bubble turbulent water*

Figure 6: Performance of M-FSK and M-FSCM in different levels of turbulence

The results of maximum data rate achieved by FSCM and FSK in turbulent water are shown in Figure 6. When temperature induced turbulence is present with an SI of 0.15, 4,8-FSCM achieves the highest data rate of around 1 Gbps. However, FSCM's performance deteriorates rapidly with stronger turbulence, and it eventually approaches that of FSK. On the other hand, FSK maintains a relatively stable performance trend. Thus, it can be concluded that FSCM has some resilience against turbulence, but its performance is similar to that of FSK under strong turbulent conditions. For the use of bubble induced turbulence, the fading experienced is different to temperature induced turbulence as illustrated in Figure 3. Thus, the performance in Figure 6a is somehow different to that reported in Figure 6b. From Figure 6b, it is observed that 4,8-FSCM achieve the highest data rate, and it can always maintain a data rate of over 1 Gbps even with increasing bubble induced turbulence. FSK has a more robust performance trend but a lower data rate with modulation levels of 4, 8 and 16. Furthermore, both FSCM and FSK exhibit a slower deterioration in performance compared to conditions of temperature induced turbulence. This indicates that the fading caused by temperature induced turbulence has a greater impact on UOWC channel than that from bubbles whose sizes are larger than the wavelength of the light beam, as described in Section 4.

6. CONCLUSION

This paper demonstrates experimental comparison of FSCM and FSK in different UOWC channel conditions using a lab-based water tank. In still water where the link performance is constrained by the limited bandwidth of the devices, FSCM is shown to achieve higher transmission speed compared to the FSK-based approach; a maximum of 1.25 Gbps compared to 850 Mbps achievable with FSK. However, in turbulence induced fading channel the FSCM technique is less resilient. Thus, FSCM will be more suitable for transmission at moderate speeds in practical UOWC systems that require resilience against channel fading.

REFERENCES

[1] Hemani Kaushal and Georges Kaddoum. “Underwater optical wireless communication”. In: *IEEE access* 4 (2016), pp. 1518–1547.

[2] Noha Anous et al. “Performance evaluation of LOS and NLOS vertical inhomogeneous links in underwater visible light communications”. In: *IEEE Access* 6 (2018), pp. 22408–22420.

[3] Callum T Geldard et al. “An empirical comparison of modulation schemes in turbulent underwater optical wireless communications”. In: *Journal of Lightwave Technology* 40.7 (2021), pp. 2000–2007.

[4] Egecan Guler et al. “A Demonstration of Frequency-Shift Keying in Underwater Optical Wireless Communications”. In: *Proceedings of Conference on Lasers and Electro-Optics*. Optica. 2022, pp. 1–2.

[5] Callum T Geldard. “Underwater optical wireless communications in turbulent conditions: from simulation to experimentation”. PhD thesis. University of Edinburgh, 2022.

[6] Mohammed Sait et al. “The impact of vertical salinity gradient on non-line-of-sight underwater optical wireless communication”. In: *IEEE Photonics Journal* 13.6 (2021), pp. 1–9.

[7] Zabih Ghassemlooy, Wasiu Popoola, and Sujan Rajbhandari. *Optical wireless communications: system and channel modelling with Matlab®*. CRC press, 2019.

[8] Lorenzo Vangelista. “Frequency shift chirp modulation: The LoRa modulation”. In: *IEEE signal processing letters* 24.12 (2017), pp. 1818–1821.

[9] Gutema Tilahun. “Enhanced Energy and Spectrum Efficiency in Visible Light Communications”. PhD thesis. University of Edinburgh, 2023.

[10] Craig A Williamson and Richard C Hollins. “Measured IOPs of Jerlov water types”. In: *Applied Optics* 61.33 (2022), pp. 9951–9961.

[11] N.G. Jerlov, F.F. Koczy, and Albatross (Schooner). *Photographic Measurements of Daylight in Deep Water*. Reports of the Swedish Deep-Sea Expedition, 1947-1948 ; v. 3: Physics and chemistry. Elanders boktr.

[12] Callum T Geldard, John Thompson, and Wasiu O Popoola. “Empirical study of the underwater turbulence effect on non-coherent light”. In: *IEEE Photonics Technology Letters* 32.20 (2020), pp. 1307–1310.

[13] Hassan M Oubei. “Underwater wireless optical communications systems: From system-level demonstrations to channel modeling”. PhD thesis. 2018.

[14] Mohammad Vahid Jamali et al. “Statistical distribution of intensity fluctuations for underwater wireless optical channels in the presence of air bubbles”. In: *2016 Iran Workshop on Communication and Information Theory (IWCIT)*. IEEE. 2016, pp. 1–6.